nature nanotechnology

SUPPLEMENTARY INFORMATION

DOI: 10.1038/NNANO.2017.190

In the format provided by the authors and unedited.

Absence of red-shift in the direct bandgap of silicon nanocrystals with reduced size

Jun-Wei Luo[1,2]*, Shu-Shen Li[1,2], Ilya Sychugov[3], Federico Pevere[3], Jan Linnros[3], and Alex Zunger[4]*

[1]*State Key Laboratory for Superlattices and Microstructures, Institute of Semiconductors, Chinese Academy of Sciences, PO Box 912, Beijing 100083, China*

[2]*Synergetic Innovation Center of Quantum Information and Quantum Physics, University of Science and Technology of China, Hefei, Anhui 230026, China*

[3]*Materials and Nano Physics Department, KTH – Royal Institute of Technology, Kista, Stockholm, 16440, Sweden*

[4]*Renewable and Sustainable Energy Institute, University of Colorado, Boulder, CO 80309, USA*

*Email: jwluo@semi.ac.cn; Alex.Zunger@Colorado.edu

Methods

Atomistic pseudopotential theory: we obtain the single-particle eigenstates $\{\epsilon_i; \psi_i(\boldsymbol{r})\}$ of the Si nanocrystals from direct diagonalization, in a basis set of plane-wave functions, of the Schrödinger equation[1]:

$$\left(-\frac{\hbar^2}{2m}\nabla^2 + V(\mathbf{r})\right)\psi_i(\mathbf{r}) = \epsilon_i\psi_i(\mathbf{r}), \qquad (1)$$

where the crystal potential of the nanocrystal plus its matrix are both described as a superposition of atomic screened (semi-empirical pseudopotential) potentials v_α of atom type at each atomic site $\boldsymbol{R}_{\alpha,n}$ within the lattice site n: $V(\boldsymbol{r}) = \sum_{\alpha,n} v_\alpha(\boldsymbol{r} - \boldsymbol{R}_{\alpha,n})$. The pseudopotentials v_α are fitted to experimental transition energies, effective masses, and deformation potentials of the bulk material[2]. This atomistic pseudopotential approach takes into account inter-band coupling, inter-valley

coupling (coupling between different parts of the Brillouin zone), and spin-orbit coupling. This approach frees us from relying on the simplified effective-mass based (continuum) approximations for describing electronic levels. The well-known density functional errors in band gaps and effective masses[3], both rather detrimental to obtaining a physically correct description of quantum confinement, were corrected by applying small adjustments in the pseudopotential in the core region. We calculated the energy states in a wide energy window from the conduction-band minimum (CBM) up to states with energy of ~ 4 eV above the bulk Si valence-band maximum (VBM) and the absorption spectra for Si nanocrystals. For the purpose of analysis only, we expand nanocrystal wavefunctions by a set of Bloch states of underlying perfect Si crystal: $\psi_i(\boldsymbol{r}) = \sum_{n,\boldsymbol{k}} c_i(n,\boldsymbol{k})\phi_{n,\boldsymbol{k}}(\boldsymbol{r})$, and we obtain the "majority representation" decomposition of the nanocrystal states by summing over the coefficients $c_i(n,\boldsymbol{k})$ to obtain the projection of the nanocrystal wave function i on each k point in the bulk Si Brillouin zone: $P_i(\boldsymbol{k}) = \sum_n |c_i(n,\boldsymbol{k})|^2$. An auxiliary quantity useful for analysis is the weight functions w_i^{Γ}, w_i^{X}, and w_i^{L}, which are defined by summing $P_i(\boldsymbol{k})$ over the $\boldsymbol{k}$ points contained in a spherical region around Γ, X, and L, respectively, as[4]:

$$w_i^{\Gamma(X,L)} = \sum_{\boldsymbol{k}\in\Omega_{\Gamma(X,L)}} P_i(\boldsymbol{k}). \qquad (2)$$

The spheres Ω_Γ, Ω_X, and Ω_L centered at Γ, X, and L in the fcc Brillouin zone have the same radius. The no-phonon optical absorption spectrum $\alpha(\hbar\omega)$ in single-particle basis is calculated, given the dipole transition matrix $\overline{P}_{vc} = < v|\hat{e}\cdot\mathbf{p}|c >$, according to the Fermi-golden rule:

$$\alpha(\hbar\omega) = \left(\frac{2\pi e}{m_0\omega}\right)^2 \sum_v \sum_c |\overline{P}_{vc}|^2 exp\left[-\left(\frac{\hbar\omega - E_{vc}}{\lambda}\right)^2\right]. \qquad (3)$$

Here, $E_{vc} = \epsilon_c - \epsilon_v$ is the transition energy from hole state v to electron state c, m_0 is the free-electron mass, and e is the free-electron charge, and λ represents the spectral line broadening.

Single-dot absorption spectroscopy: Photoluminescence excitation experiment was performed on Si nanocrystals embedded in a silica matrix prepared from thin

silicon-on-insulator wafers by thermal oxidation (900°C for 30 seconds) [5]. Silicon dioxide thickness was 1.1 μm. Nanocrystals are close to spherical or faceted in shape as revealed by TEM imaging [6]. A laser-driven Xe lamp with an attached monochromator ensured stable and tunable excitation with ~ 6 nm spectral bandwidth (20-60 meV in the experimental energy range). A thermoelectrically cooled (-100 °C) CCD camera with electron gain was used to detect weak single-dot luminescence in epifluorescence configuration with a wide-field microscope. To obtain the absorption spectra the measured photoluminescence signal was corrected for the excitation power recorded for each excitation wavelength. To calibrate obtained absorption curves a modulated excitation by a 405 nm laser diode was used, where the luminescence rise time provided information of the absolute value of the absorption cross-section [7]. The single dot absorption spectra reveal several prominent peaks. Optical interference effects can be ruled out due to poor temporal and spatial coherence of the excitation light at the sample position. The 6 nm bandwidth of the spectrally-filtered lamp corresponds to ~ 20 μm coherence length, while here the beam travelled 2-3 meters to the sample. Since the beam was expanded to a several mm waist and then focused to a ~ 30 μm spot to feed it to the sample through the microscope the lateral (spatial) coherence is also destroyed. As a practical manifestation we note that different numerical aperture objective lenses were used for room and low temperature measurements (0.9 and 0.75, respectively). Those would be expected to produce different interference patterns because of different effect on lateral coherence, but instead we see a consistent absorption structure at both temperatures[8]. These peaks were identified via the atomistic calculations to originate from the indirect band edge X-dominated excited states with enhanced Γ mixing (Figure 1b). Peak positions and linewidths of four deconvoluted peaks from the absorption spectra of nine different Si nanocrystals and are shown in Figure S1. By comparison with atomistic calculations, we identify the first peak in the experimental absorption curve at ~ 2.3 eV as a combination of $S_h \rightarrow D_e$ and $P_h \rightarrow P_e$ transitions, while the next broad peak at ~ 2.65 eV partially consists of $P_h \rightarrow D_e$ family of transitions. These corresponding wavefunctions are given in our previous work [2]. Identified theoretical quantum dot

transitions also do not reveal strong size-dependence in the given energy interval (lines in Figure S1).

Extended discussions

Truncated crystal approximation extracting nanocrystal levels from the bands of the periodic bulk crystal predicted red-shift of direct edge: A more advanced method to guess the nanocrystal levels from bulk properties, as done in effective mass theories, was attempted by Krishna and Friesner [9] who used the nonparabolic dispersion of the 3D *bulk* band structure of crystalline Si to deduce the expected energy levels *vs* size in Si 0D nanocrystals. Given the curvatures of the bulk band structure shown in Fig. S2 they proposed a blue-shift of the direct band gap that changes over to a red shift at extremely small nanocrystal sizes of about 0.4 nm [9]. Again, the direct calculation on Si nanocrystal (not relying on the bulk band structure alone to deduce nanocrystal levels) does not give this result.

Alternative explanations for the red moving band are possible: The present work rules out the existence of a red-shifted band arising from the direct band gap transition. We propose instead an alternative explanation of the effect observed in Ref. 10. State filling facilitated by strong pumping with subsequent fast recombination of multiexcitons can be responsible for the measured emission, which has been demonstrated for Si nanocrystals in Ref. 11. The red-shift would then correspond to the multi-exciton depopulation due to enhanced recombination rate at the fundamental band gap of smaller nanocrystals. This would lead to a red-shifted spectrum for the hot PL as higher states are emptied faster for smaller nanocrystals. Thus, the nanosecond-fast, "direct-like" recombination observed in Ref. 10, could be an effect of Auger or multi-exciton recombination, not a shifting of the Γ-energy. An interpretation consistent with that is that this hot PL is only observed at high excitation conditions (n >1). Another possible alternative assignment of the observed

red-shifted PL peak by de Boer *et al.* is a radiative channel from surface localized states. In our previous work[12,13], we have shown that the surface of Si nanocrystals embedded in an oxide matrix can contain numerous interface defects that strongly affect the Si nanocrystal photoluminescence efficiency. Specifically, red-shift of PL band arising from surface-defect related transitions was observed in several experiments[14-16]. Owing to the small joint density of states of surface defect related transitions, these transitions are usually masked by Γ-X mixing enhanced band-to-band intrinsic transitions and are hardly been observable in absorption spectrum of Si nanocrystals[11] (see also Fig. 1b in main text). Therefore, it is generally accepted whether the origin of high efficient PL from extrinsic localized defect states or not, they are always present in Si nanocrystals and may affect their high excited transitions. Finally, we note the very good agreement between the single-dot absorption spectrum and the atomistic calculations (Fig. 1b in main text) over several orders of magnitude confirming the high degree of accuracy for these calculations.

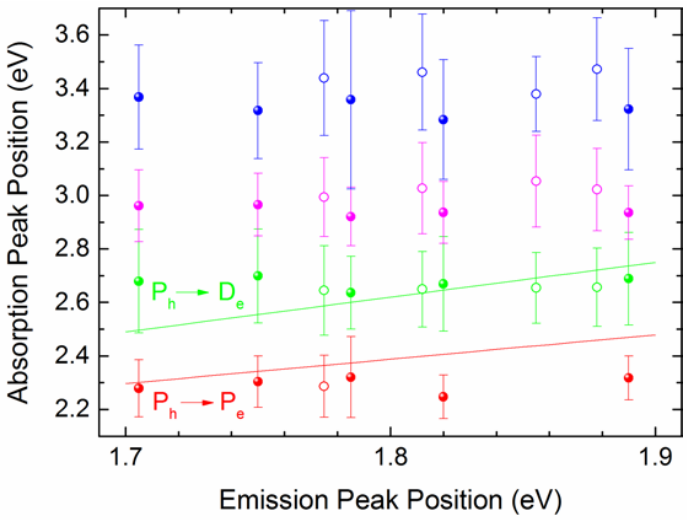

Figure S1. Positions of detected absorption peaks as a function of emission energy for 9 nanocrystals measured at room temperature (open circles) and at 70 K (filled circles). Error bars represent width of the measured peaks obtained by deconvolution. Lines show calculated energy dependence for some identified quantum dot transitions.

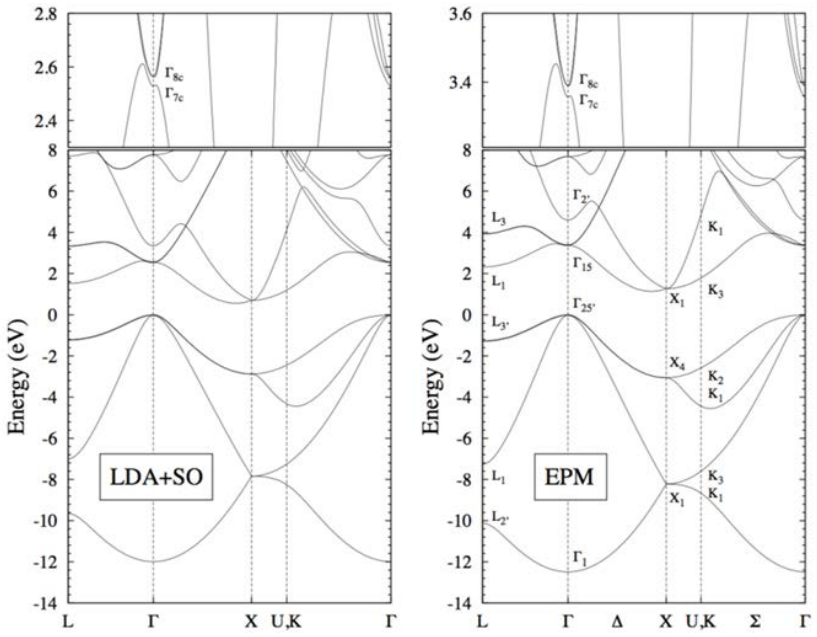

Figure S2. Comparison of band structure for bulk Si between first-principles local density approximation (left) and atomistic semi-empirical pseudopotential method (EPM) (right), including treatment of spin-orbit coupling. Top panels zoom in the band structure near conduction band at Γ-valley.

References:

1 Wang, L.-W. & Zunger, A. Solving Schrodinger's equation around a desired energy: Application to silicon quantum dots. *The Journal of Chemical Physics* **100**, 2394-2397, doi:10.1063/1.466486 (1994).

2 Luo, J.-W., Stradins, P. & Zunger, A. Matrix-embedded silicon quantum dots for photovoltaic applications: a theoretical study of critical factors. *Energy & Environmental Science* **4**, 2546-2557 (2011).

3 Wang, L. W. & Zunger, A. Local-density-derived semiempirical pseudopotentials. *Physical Review B* **51**, 17398-17416 (1995).

4 Wang, L. W., Bellaiche, L., Wei, S. H. & Zunger, A. Majority Representation of Alloy Electronic States. *Physical Review Letters* **80**, 4725-4728 (1998).

5 Sychugov, I., Nakayama, Y. & Mitsuishi, K. Sub-10 nm crystalline silicon nanostructures by electron beam induced deposition lithography. *Nanotechnology* **21**, 285307 (2010).

6 Sychugov, I., Valenta, J., Mitsuishi, K., Fujii, M. & Linnros, J. Photoluminescence measurements of zero-phonon optical transitions in silicon nanocrystals. *Physical Review B* **84**, 125326 (2011).

7 Sangghaleh, F., Bruhn, B., Sychugov, I. & Linnros, J. Optical absorption cross section and quantum efficiency of a single silicon quantum dot. *Proc. of SPIE* **8766**, 876607 (2013).

8 Sychugov, I., Pevere, F., Luo, J.-W., Zunger, A. & Linnros, J. Single-dot absorption spectroscopy and theory of silicon nanocrystals. *Physical Review B* **93**, 161413 (2016).

9 Krishna, M. V. R. & Friesner, R. A. Prediction of anomalous redshift in semiconductor clusters. *The Journal of Chemical Physics* **96**, 873-877 (1992).

10 de Boer, W. D. A. M. *et al.* Red spectral shift and enhanced quantum efficiency in phonon-free photoluminescence from silicon nanocrystals. *Nat Nano* **5**, 878-884 (2010).

11 Sykora, M. *et al.* Size-Dependent Intrinsic Radiative Decay Rates of Silicon Nanocrystals at Large Confinement Energies. *Physical Review Letters* **100**, 067401 (2008).

12 Sangghaleh, F., Bruhn, B., Schmidt, T. & Linnros, J. Exciton lifetime measurements on single silicon quantum dots. *Nanotechnology* **24**, 225204, doi:10.1088/0957-4484/24/22/225204 (2013).

13 Lee, B. G. *et al.* Strained Interface Defects in Silicon Nanocrystals. *Advanced Functional Materials*, n/a-n/a, doi:10.1002/adfm.201200572 (2012).

14 Dohnalová, K., Gregorkiewicz, T. & Kůsová, K. Silicon quantum dots: surface matters. *Journal of Physics: Condensed Matter* **26**, 173201, doi:10.1088/0953-8984/26/17/173201 (2014).

15 Biteen, J. S., Lewis, N. S., Atwater, H. A. & Polman, A. Size-dependent oxygen-related electronic states in silicon nanocrystals. *Applied physics letters* **84**, 5389-5391 (2004).

16 Wolkin, M. V., Jorne, J., Fauchet, P. M., Allan, G. & Delerue, C. Electronic States and Luminescence in Porous Silicon Quantum Dots: The Role of Oxygen. *Physical Review Letters* **82**, 197-200 (1999).